Characterization of Pt-impregnated MCM-41 and MCM-48 and their catalytic performances in selective catalytic reduction for NO_x

D-J Kim , J-K Cho, J-H Jang, S-C Lee, M Kang[1], and S-J Choung[*]

Department of Chemical Engineering, School of Environmental Applied Chemistry,

Kyung Hee University, Yongin, Gyeonggi, 449-701, South Korea

[1]*Industrial Liaison Research Institute, Kyung Hee University, Yongin, Gyeonggi 449-701, South Korea*

*Corresponding author: E-mail address: sjchoung@khu.ac.kr, Fax: +82-31-202-4765, Tel: +82-31-201-2971

[1]Co-corresponding author: E-mail address: mskang@khu.ac.kr, Fax: +82-31-202-4765, Tel: +82-31-201-2121

Abstract

This study has been focused on the comparison of de-NO_X mechanisms and surface physical properties between Pt impregnated MCM-41 and MCM-48 with different framework dimension. In de-NO_X reaction, the NO reduction occurred from 250 °C with reducing reagent (propylene) combustion in both catalysts. However the conversion has the maximum (60%) at 300 °C in case of Pt/MCM-41, otherwise it enhanced, and in addition, kept to high temperature of 550 °C without conversion decrease in Pt/MCM-48. This result must be attributed to the difference of structural dimension, surface acidity, adsorption abilities of reducing agent and NO, and finally the different Pt active species on MCM-41 and MCM–48. The adsorption ability for NO, reducing agent (propylene), and NH_3 definitely increased on Pt/MCM-48 compared with Pt/MCM-41. In XPS and XRD results, it suggested that the PtO and PtO_2 have been role as active species on Pt/MCM-48, while the PtO only presented on Pt/MCM-41. From results of physical properties mentioned and *in-situ* IR spectra, it could be supposed that the de-NOx reaction in Pt/MCM-41 was progressed by partially oxidation and reduction for reducing agent and NO, respectively, as resulting in produce NCO and $C_xH_yO_z^*$ intermediates, however, it was occurred though the completely oxidation and reduction of these on Pt/MCM-48.

1. Introduction

Selective catalytic reduction of NOx in oxygen rich exhaust stream of stationary and mobile is one of the major challenges in environmental catalysis. Ever since Iwamoto et al. [1, 2] reported that transition metal ion exchanged zeolites, in particular Cu-ZSM-5, showed high HC-SCR activity, a number of weak has been published reporting the catalytic behavior of those catalysts [3, 4]. However, due to the poor hydrothermal stability and low activity of transition metal ion exchange zeolites in the presence of H_2O and SO_2 they are unlikely to be practical catalyst for lean NOx abatement. After that, the Pt based catalysts (Pt supported on TiO_2, SiO_2, ZrO_2, Al_2O_3 and ZSM-5) reported to have the high resistance against SO_2 and H_2O vapor [5 - 9], and then they have been focused to be the most promising catalyst for selective catalytic reduction of NOx.

On the other hand, the metal oxides and microporous materials as a support were used in SCR process until now. However, the application has a limitation to use in industrial division because of limitation of metal impregnation due to lower surface area, the diffuse resistance of reactant due to narrow or small pore size, and low hydrothermal stability. Therefore, to solve these problems, it is need to the larger porous support. And then, mesoporous materials have been introducing, in addition MCM-41 with hexagonal straight tunnel of two-

dimensional structure. This material should be expected to useful for the high dispersion of active species and easy diffusion, and high hydrothermal stability because of higher surface area and lager pore size [10 - 12]. As the result, Pt/MCM-41 catalyst has been reported to have high activity for NO reduction by propylene, and provided the highest specific NO reduction rates for Pt as compared with Pt supported on all other conventional supports [13 - 14]. Excepting MCM-41, however, the few paper written about other mesoporous materials for application to de-NOx have been reported until now.

In this study, the Pt-impregnated mesoporous materials (Pt/MCM-41 and Pt/MCM-48) of two types with different structural dimensions are applied to de-NOx reaction of SCR process, and were characterized by various measurements. In particular, we have tried to find out the difference of pathway in de-NOx process resulting from different physical properties, which were generated by introduce of two supports. In addition, the *in-situ* FT-IR measurement was also done to find out the mechanism in de-NOx process in this study.

2. Experimental

2.1. Preparation of catalyst

The mesoporous silicate materials were prepared by a commonly hydrothermal method [15, 16]. First, MCM-41 synthesis follows the next: The Ludox HS 40 colloidal silica (40 wt% SiO_2, Dupont) as a silica source was added in mixing solution of sodium hydroxide (NaOH, 99.9%, Aldrich.) and distilled water. The cetylmetylammonium chloride (HTACl, 25 wt%, Aldrich) as a template was slowly dropped into in this solution. The composition of final sol solution was $6.0SiO_2$: 1.0HTACl : $1.5Na_2O$: $0.15(NH_4)_2O$: $350H_2O$. The pH was fixed to 11 and the crystallization was done at 100°C for 48 h. Attained powder was washed, filtered, and then calcined at 550 °C for 12 h in air condition. On the other hand, the synthesis of MCM-48 was the same to that of MCM-41 excepting use of cetylmetylammonium bromide (HTABr, 99.99%, Aldrich) and LE-4 as templates. The composition of final solution was $5.0SiO_2$: 0.85HTABr : 1.25LE-4 : $400H_2O$. Finally, the platinum to generate activated sites was impregnated on the mesoporous surface by a dry method, and the amount was fixed to the 1.0 wt-% of total catalytic amount.

2.2. Characterization

Prepared catalysts were identified through powder X-ray diffraction analysis (XRD, model PW 1830 from Philips) with nickel-filtered CuK_a radiation (40 kV, 100 mA) at 2-theta angle of 5 - 70˚. The scan speed was 10 ˚/min and the time constant 1sec.

Catalysts BET surface and pore size distribution (PSD) were measured using Micrometrics ASAP 2000. All catalysts were degassed before BET surface and PSD measurement. The degassing was carried out under vacuum at 393 K for 3 h and then at 573 K for 5 h for each sample.

Temperature programmed technique is explained the next: about 0.2g of catalyst were pretreated under He flow (30 ml/min) at 550 °C for 2 h, and then cooled to room temperature. Each absorber (NH_3, C_3H_6, and NO) adsorptions were then performed at room temperature by flowing 30 ml/min of absorbers/He for 1 h. Afterwards, absorbers in the gas phase were removed with He (30 ml/min) until no absorbers were detected in the effluent. The desorption experiments were then carried out from room temperature to 550 °C, at 5 °C /min, under He flow. The compositions of gases desorbed from catalysts were monitored by using a TCD (GC series 580, GOW-MAC).

To analysis of binding energy between Pt4f and Ols, the X-ray photoelectron spectroscopy (XPS,

PHI 5700, PHI com.) was employed. The fresh catalysts were prepared with pellets of 5 mm and treated in vacuum overnight prior to the measurement. The Al mono (pass energy = 23.5 eV) was used as X-ray source at 350 W power, 15 kV, and pressure of below 2.7 x 10^{-6} Pa during the measurement.

In-situ FT-IR spectra test follows the next: Infrared spectra were collected using a Shimazu FTIR-8400 fourier transform infrared spectrometer 20.0 mg of catalyst sample was pressed (at a pressured of 4 ton/㎠) into a self-supported wafer. An IR cell with CaF_2 windows cooled by flowing water was used. A heating wire, which was wrapped around ceramics near the sample wafer, allowed collection of *in-situ* spectra at room temperature ~ 400 ℃. The temperature was monitored though a thermocouple located in the cell and in close proximity with the catalyst sample. Gas mixtures concentration used in this study was 1000 ppm of NO, 1000 ppm of C_3H_6, and 2.5 vol.-% of O_2. Gases were mixed at appropriate amounts and introduced to the IR cell using a system of mass flow meters and needle valves. The volumetric flow rate of the gas mixtures was held at 50 ml/min.

H_2-TPR (temperature programmed reduction) was the follows: About 0.3g of catalysts were pretreated under He flow (30 ml/min) at 550 ℃ for 2 h, and then cooled to room temperature. Analysis was carried out by flowing 30 ml/min of H_2 (10 vol.-%)/N_2 and raising the catalysts temperature from room temperature to 550 ℃ at 5 ℃/min. The change in hydrogen concentration was measure by a gas chromatograph (GC series 580, GOW-MAC) equipped with a TCD.

3. Results and discussion

3.1. Physical properties for prepared Pt/MCM-41 and Pt/MCM-48

The mesoporous structure of catalysts are identified by XRD as shown in Fig. 1, the samples displayed a well-developed mesoporous structure MCM-41 (two-dimension hexagonal straight pore) and MCM-48 (three dimensional pore). The impregnated Pt oxidation states are different on MCM-41 and MCM-48: the only Pt^{2+}(PtO) in MCM-41, otherwise, Pt^{2+}(PtO) and the Pt^{4+}(PtO_2) in MCM-48. This result means that the Pt species impreganated were higher dispersed on MCM-48 than on MCM-41.

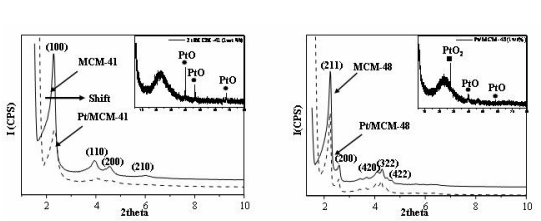

Catalyst	BET specific Surface area(m^2/g)	Pore volume (cc/g)	Pore size (Å)
MCM-41	1098	0.8	29
MCM-48	1054	1.0	32
Pt/MCM-41	1012	0.8	27
Pt/MCM-48	1043	1.1	30

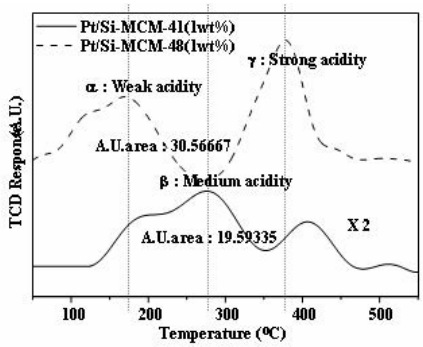

Fig. 1. XRD patterns and BET surface areas of Pt/MCM-41 and Pt/MCM-48. a) Pt/MCM-41 and Pt/MCM-48

Fig. 2. NH_3-TPD curves of Pt/MCM-41 and Pt/MCM-48.

Fig. 2 shows the NH_3-TPD curves of Pt/MCM-41 and Pt/MCM-48. In general, these profiles for microstructure consist of two peaks; one appears at a low temperature range around 150 ~ 200 ℃ and another

appears at a high temperature range around 350 ~ 450 ℃. The low and high temperature peaks correspond to the weak and strong acid sites, respectively. In this study, three pattern for NH_3 desorption appeared; the first curve due to the adsorbed NH_3 on pure mesoporous surface and the second and third curves by the NH_3 adsorption on the impregnated different Pt species on MCM-41 and 48.

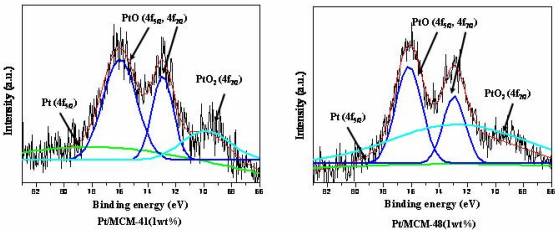

Catalysts	Pt/MCM-41			Pt/MCM-48		
Pt species	Pt	PtO	PtO_2	Pt	PtO	PtO_2
Peak area (a.u.)	0.41	1.0	0.44	0.33	1.0	0.69

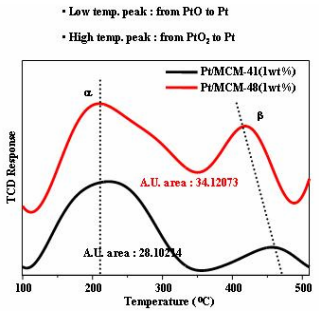

Fig. 3. X-ray photoelectron spectra of in Pt/MCM-41 and Pt/MCM-48. a) Pt/MCM-41 and b) Pt/MCM-48

Fig. 4. H_2-TPR curves of in Pt/MCM-41 and Pt/MCM-48.

Fig. 3 shows XPS spectra for Pt4f orbital impregnated on MCM-41 and MCM-48. The binding energies were displayed in four-type peaks, which shown at 80, 77, 73, and 70 eV assigned to $Pt4f_{5/2}$, $PtO4f_{5/2}$, $PtO4f_{7/2}$, and $PtO_24f_{7/1}$, respectively [17, 18]. This result means that the PtO_2 species, which can be role as a active sites in de-NOx, much present on surface of MCM-48. This result was well matched to the XRD result mentioned up. Maybe, the more oxidized PtO_2 will completely oxidize the propylene of reducing agent, than PtO, resulted to give the different de-NOx mechanism.

Fig. 4 shows the H_2-reduction curves of Pt species impregnated on MCM-41 and MCM-48. We have already suggested that the active sites were different in Pt/MCM-41 and Pt/MCM-48 in XRD and XPS results. From this result, it could be supposed that the Pt active sites present at high temperature in MCM-48, resulting to keep the high NO conversion at high temperature. Maybe, the PtO_2 active site has role to progress de-NO_x at high temperature in Pt/MCM-48. On the other hand, the curve disappeared at high temperature in Pt/MCM-41.

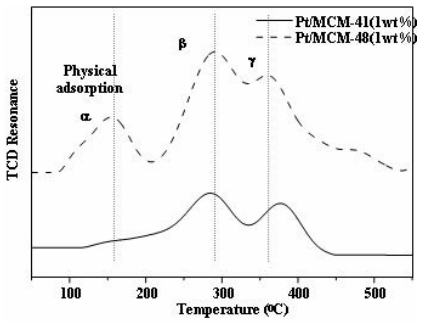

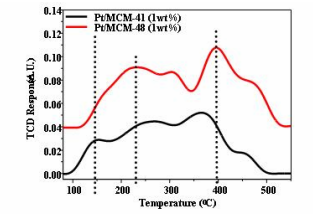

Sample	Peak	Activation energy E(kcal/mol)
Si-MCM-41	first	4.57
	second	3.24
Si-MCM-48	first	4.34
	second	3.04

$\log\Phi + \frac{0.456E}{RT_m} = \text{constant}$

Φ = heating rate (℃/min)
R = gas constant
T_m = maximum deflection temperature
E = activation energy

Fig. 5. Etylene desorption curves and activation energies calculated from Ozawa methodfor water desorption in Pt/MCM-41 and Pt/MCM-48.

Fig. 6. NO-TPD curves in Pt/MCM-41 and Pt/MCM-48.

3.2. Adsorption ability for reactant of Pt/MCM-41 and Pt/MCM-48

In general, it was well known that the catalytic performance in de-NOx reaction strongly related to

adsorption ability NO and reducing agent. The more adsorption ability increased, the catalytic activity also increased. The NO desorption patterns were also similar to the NH_3-TPD curves as three types as shown in Fig. 5. The NO adsorption ability, in particular, more enhanced at high temperature in Pt/MCM-48 compared to the Pt/MCM-41, however the adsorption amount at low temperature was very small in both catalysts, and then was ignored. This result also explains that the NO conversion will be increased at high temperature in Pt/MCM-48.

The adsorption abilities of propylene added as a reducing regent are displayed in Fig. 6. Three-type curves also appeared as like in NH_3 and NO-TPD curves. However, the adsorption appeared in all temperature range, differently to the NO adsorption patterns. At low temperature, the adsorption abilities were resemble in both catalysts. From the results of NO and C_3H_6-TPD, we could assumed that the NO conversion activity will be enhanced in Pt/MCM-48 compared with in Pt/MCM-41, and in addition, the pathway from NO to N_2 in de-NOx process will be different in both catalysts. On the other hand, the activation energy for water desorption was compared in under table. The Ozawa presented a useful equation to calculate the activation energy as shown in here. Ozawa have presented a useful equation to calculate the activation energy of various thermal reactions based on the shifts of the maximum deflection temperature T_m of DSC curves upon the changing of heating rates [19, 20].

$\text{Log } \phi + 0.4567E/RT_m = \text{constant}$

Here ϕ : heating rate, T_m : maximum deflection temperature, E : activation energy, R : gas constant. The activation energy can be derived from the slope, 0.4567E/R from the plot of log verse $1/T_m$. This experiment is often used to discuss the hydrophilic property of structure. Generally the propylene molecule and water are competitively adsorbed on the surface of materials. Consequently, if the water desorption activation energy increase, the propylene adsorption of reducing agent relatively decrease. As shown, the energy is more weak in Pt/MCM-48 compared with Pt/MCM-41.

3.3. Catalytic performance for selective catalytic reduction on NO

Fig. 7 shows the effect of reaction temperature in de-NOx reaction on Pt/MCM-41 and Pt/MCM-48. As shown, the NO reduction simultaneously occurred with propylene combustion from 250 ℃ in both catalysts. However, the NO conversions displayed 60% and 80% as the maximum, however, the higher NO conversion (80%) was surprisingly kept in Pt/MCM-48 to high temperature region, while the NO conversion (60%) rapidly decreased in Pt/MCM-41 after 350 ℃. This was attributed to the different NO and propylene adsorption ability as the mentioned. On the other hand, in case of propylene conversion, it rather reached 80% in Pt/MCM-41 compared with 50% in Pt/MCM-48. This result means that the Pt species impregnated on MCM-48 are easily reduced by the smaller propylene compared with Pt species on MCM-41, therefore, the need propylene amounts for NO reduction was smaller in Pt/MCM-48.

The optimum ratios of HC/NO were 0.5 and 1.0 in Pt/MCM-48 and 41, respectively, and the conversion was not enhanced in both catalysts although the increase of HC/NO ratio. The reason for difference of reducing agent amount also could be explained to the difference of Pt active species in Pt/MCM-41 and Pt/MCM-48, as the mentioned in Fig. 7.

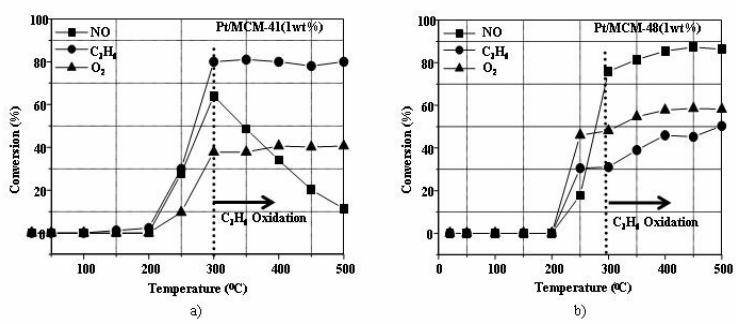

Fig. 7. Catalytic performance on de-NOx reaction in Pt/MCM-41 and Pt/MCM-48.
a) Pt/MCM-41 and b) Pt/MCM-48

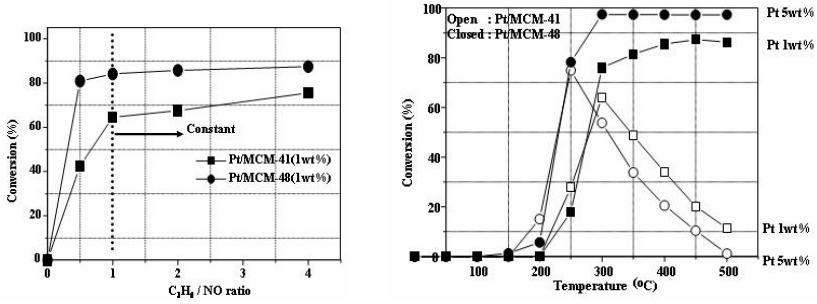

Fig. 8. Relationship between the NO conversion and C_3H_6/NO ratio.

Fig. 11. Catalytic performance of de-NOx reaction with Pt loading amount in Pt/MCM-41 and Pt/MCM-48.

3.4. Suggestion of de-NO_X mechanism from in-situ FT-IR spectrum during de-NOx reaction

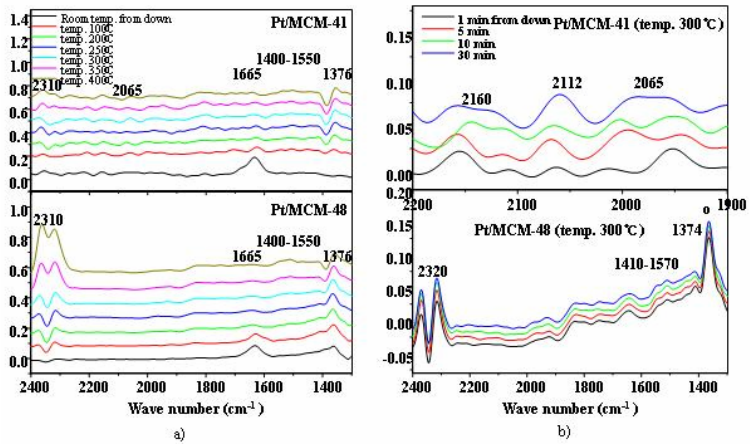

Fig. 11. *In-situ* FT-IR spectra during de-NOx reaction in Pt/MCM-41 and Pt/MCM-48.

a) Under NO + C_3H_6 + O_2 and b) Under NO + C_3H_6 + O_2 at 300℃.

To know the mechanism of de-NOx in Pt/MCM-41 and Pt/MCM-48, the produced intermediates during de-NOx reaction were analyzed by *in-situ* FT-IR method, and the result is shown in (a) and (b) of Fig. 11. The IR bands could be assigned to the next [21, 22]: partial oxidized C_3H_6 band of 1400-1500 cm^{-1}, gas phase C_3H_6 or gas phase NO band of 1665 cm^{-1}, CO band of 2065 cm^{-1}, and CO_2 band of 2310 cm^{-1}. In particular, the 2065, 2112, and 2160 cm^{-1} bands could be assigned the CO, CN, and NCO bands in (b), respectively. In case of Pt/MCM-41, the NO and C_3H_6 bands decreased and CO_2 was not changed with an

increase of reaction temperature. At 300 ℃ of optimum reaction temperature in (b), the CO, CN, and NCO bands were showed in Pt/MCM-41, but theses bands was not appeared in Pt/MCM-48. Therefore, we supposed from these results that the mechanisms and the active sites for de-NOx in Pt/MCM-41 and Pt/MCM-48 must be different. From FT-IR and XPS results, we have also try to mention about the difference of de-NO_X mechanism in Pt/MCM-41 and Pt/MCM-48, simply. In Pt/MCM-48, the reducing agent was completely oxidized to CO_2, and then it easily reduced PtO_2 of active sites in Pt/MCM-48. Therefore, the NO directly reduced to N_2 without NCO intermediate formation in Pt/MCM-48.

4. Conclusion

1. In NH_3-TPD result, the total acidic amount; Pt/MCM-48 >> Pt/MCM-41. **2**. The adsorptions NO and reduce agent amount of Pt/MCM-48 increased at high temperature compared to Pt/MCM-41. **3**. From XPS and in-situ FT-IR results, it was identified that Pt species impregnated on MCM-41 and MCM-48 was different, resulting to the different reaction mechanism in de-NO_X process.

References

[1] M. Iwamoto, H. Frukawa, Y. Mine, F. Uemura, S. Mikuriya, S. Kagawa, J. Chem. Soc. Chem. Commun. (1986) 1272.

[2] M. Iwamoto, H. Yahiro, Y. Yu-u, S. Shundo, N. Mizuno, Shokubai 32 (1990) 430.

[3] A. P. Walker, Catal. Today 26 (1995) 107.

[4] J. Y. Yan, G. -D. Lei, W. M. H. Sachtler and H. H. Kung, J. Catal. 161 (1996) 43.

[5] R. Burch, P. J. Millington and A. P. Walker, Appl. Catal. B 4 (1994) 65.

[6] R. Burch and T. C. Watling, Catal. Lett. 43 (1997) 19.

[7] T. Tanaka, T. Okuhara and M. Misono, Appl. Catal. B 4 (1994) L1.

[8] G. R. Bamwenda, A. Ogata, A. Obuchi, J. Oi, K. Mizuno and J. Skrzypek, Appl. Catal. B 6 (1995) 311.

[9] Mei Xin, In Chul Hwang, Do Heui Kim, Se In Cho and Seong Ihl Woo, Appl. Catal. B 21 (1999) 183.

[10] S. -C. Shen and S. Kawi, Catal. Today 68 (2001) 245.

[11] R. Long and R. T. Yang, Catal. Lett. 52 (1998) 91.

[12] Jong Yeol Jeon, Hee Young Kim and Seong Ihl Woo, Appl. Catal. B 44 (2003) 311.

[13] Dinyar K. Captain and Michael D. Amiridis, J. Catal. 184 (1999) 377.

[14] J. M. García-Cortés, J. Pérez-Ramírez, M. J. Illán-Gómez, F. Kapteijn, J. A. Moulijn and C. Salinas-Martínez de Lecea, Appl. Catal. B 30 (2001) 399.

[15] M. L. Peña, Q. Kan, A. Corma and F. Rey, Micro. & Meso. Mater. 44 (2001) 9.

[16] D. Zhao and D. Goldfarb, J. Chem. Soc. Chem. Commun. 8 (1995) 875.

[17] G. Kiss, V. K. Josepovits, K. Kovacs, B. Ostrick, M. Fleischer, H. Meixner, F. Reti, Thin Solid Films 436 (2003) 115.

[18] H. Karhu, A. Kalantar, I. J. Vayrynen, T. Salmi and D. Yu. Murzin, Appl. Catal. A 247 (2003) 283.

[19] T. Ozawa, J. Therm. Anal. 5 (1973) 563.

[20] M. Kang, S.-Y. Lee, C.-H. Chung, S. M. Cho, G-Y. Han, B.-W. Kim and K. J. Yoon, J. Photochem. Photobiol A 144 (2001) 185.

[21] S. -C. Shen and S. Kawi, J. Catal. 213 (2003) 241.

[22] Walter Schießer, Hannelore Vinek and Andreas Jentys, Appl. Catal. B 33 (2001) 263.